

**Title page**

**Title: Evaluation of motion correction methods for dual gated cardiac PET-CT imaging**

**Short title: Motion correction methods for dual gated cardiac PET-CT imaging**

Riku Klén<sup>1,2</sup>, Tommi Nojonen<sup>1,3</sup>, Juha Koikkalainen<sup>4</sup>, Jyrki Lötjönen<sup>4</sup>, Kris Thielemans<sup>5,6</sup>, Erika Hoppela<sup>1</sup>, Hannu Sipilä<sup>1</sup>, Mika Teräs<sup>7,8</sup>, Juhani Knuuti<sup>1</sup>

<sup>1</sup>Turku PET Centre, Turku University Hospital and University of Turku, Finland

<sup>2</sup>Department of Mathematics and Statistics, University of Turku, Finland

<sup>3</sup>Department of Nuclear Medicine, Turku University Hospital, Finland

<sup>4</sup>Knowledge Intensive Services, VTT Technical Research Centre of Finland, Finland

<sup>5</sup>Hammersmith Imanet Ltd, London, United Kingdom

<sup>6</sup>University College London, London, United Kingdom

<sup>7</sup>Department of Medical Physics, Turku University Hospital, Finland

<sup>8</sup>Institute of Biomedicine, University of Turku, Finland

Corresponding author: Riku Klén, Department of Mathematics and Statistics, 20014

University of Turku, Finland, riku.klen@utu.fi

## **Abstract and keywords**

### **Abstract**

Dual gating is a method of dividing the data of a cardiac PET scan into smaller bins according to the respiratory motion and the ECG of the patient. It reduces the undesirable motion artefacts in images but produces several images for interpretation and decreases the quality of single images. By using motion correction techniques, the motion artefacts in the dual gated images can be corrected and the images can be combined into a single motion-free image with good statistics. The aim of the present study is to develop and evaluate motion correction methods for cardiac PET studies.

We have developed and compared two different methods: CT-PET-based and CT-only methods. The methods were implemented and tested with a cardiac phantom and three patient datasets. In both methods, anatomical information of CT images is used to create models for the cardiac motion.

In the patient study the CT-only-method reduced motion (measured as the centre of mass of the myocardium) on average 43%, increased contrast-to-noise ratio on average 6.0% and reduced the target-size on average 10%. Slightly better figures (51%, 6.9% and 28%) were obtained with the CT-PET-based method. Even better results were obtained in the phantom study for both the CT-only-method (57%, 68% and 43%) and the CT-PET-based method (61%, 74% and 52).

We conclude that using anatomical information of CT for motion correction of cardiac PET images, both respiratory and pulsatile motions can be corrected with good accuracy.

**Keywords:** motion correction, cardiac PET imaging, dual gating

## **Text**

### **1. Introduction**

Small anatomical targets close to the heart, such as vulnerable coronary plaques, cardiovascular tumours or focal inflammations include diagnostically valuable information in cardiovascular images. There have recently been attempts to use positron emission tomography (PET) to image vulnerable coronary plaques [1, 2, 3]. In general motion artefacts are one of the most severe factors decreasing the quality of cardiac PET images. A few centimetres pulsatile and respiratory motion of the heart [4, 5] reduces spatial resolution in cardiac PET images which makes it difficult to detect and localise these millimetre-size targets. To make these small targets visible motion correction of cardiac PET images is crucial. The object of this study is to develop such a motion correction method for clinical purposes.

Duration of nuclear medicine scans such as PET scans are typically much longer than the duration of computed tomography (CT) scans. Due to the long acquisition time respiratory motion cannot be eliminated by breath holding. In PET studies gating is the most common method to decrease the cardiac and respiratory motion artefacts. In gated acquisition, data is divided into shorter time intervals using motion information derived, e.g., from respiratory or electrocardiography (ECG) signals. To obtain cardiac PET images with minimum amount of motion interferences, those images need to be acquired using dual gating, i.e., gated simultaneously with respect to respiratory and pulsatile motion [3, 6, 7, 8, 9].

By dual gating a number of images are created at different phases of pulsatile and respiratory cycles with less motion artefacts but also with much lower statistics than in the non-gated image. To increase the statistics, the gated images need to be summed. Before the images can be summed the motion between them has to be corrected to preserve a high spatial resolution and to achieve the best possible contrast-to-noise ratio (CNR).

Motion correction methods for PET can be divided into image-based and list-mode-data-based methods. The simplest image based motion correction methods are rigid and affine transformations, which alone do not sufficiently correct the motion artefacts in cardiac PET studies [10, 11, 12]. These methods are suitable for motion correction of objects with little deformation. There are various non-rigid motion correction methods studied such as the optical flow algorithm [13, 14, 15], the elastic transformations [16], MRI-based correction methods [17, 18] and cardiac shape tracking [19]. However, none of these techniques have utilised the dual gating in PET data processing. Recently, the different motion correction methods for dual gated cardiac PET images were studied with the list-mode data based method. [20]. That study suggests that the most efficient method for cardiac PET motion correction is to use an elastic model for each dual gated image independently. However, all these reported methods, apart from MRI based technique, implement the motion correction utilising only the PET images.

In this study we introduce motion correction methods for cardiac PET, which employ gated CT images. This is possible in PET/CT scanners in which the CT image is routinely acquired to provide precise anatomical localisation for the distribution of radiopharmaceuticals and for the attenuation correction of PET data [21]. We developed and evaluated two different image correction methods to compensate both pulsatile and

respiratory motions in cardiac PET images. Both of these methods use motion information obtained from respiratory gated CT images. Other our method employs also ECG gated CT images. . In our approach the CT images are used to create the model of respiratory and/or pulsatile motion of heart and utilised to correct these motion artefacts in cardiac PET images. These novel methods make motion correction of dual gated cardiac images possible producing corrected images with higher spatial resolution and with better CNR.

## **2. Materials and Methods**

### *2.1 Phantom and patient data acquisition*

All CT and PET data in patient and phantom studies were acquired with a Discovery VCT PET/CT scanner (GE Healthcare) [22] at Turku PET Centre. The phantom data were collected using a realistic heart phantom with simulated respiratory and pulsatile motion. The phantom described in details in [3] consisted of two nested balloons filled with water. The volume of the inner balloon was varied simulating the pulsatile motion. The phantom included four active targets representing coronary plaques. The activity of  $^{18}\text{F}$ -FDG in the targets was 1, 2, 3 and 6 kBq and the activity of the volume between the outer and inner balloons, representing myocardium, was 0.2 kBq/ml. A container including the balloons was moved back and forth to mimic respiratory motion. The purpose of this phantom study was to verify the function of dual gating and motion correction methods. Also parameters for the low-dose ECG-gated CT scan were tested to

minimise the radiation dose in the patient study. The ECG-gated CT scan was used to image pulsatile motion in phantom and patient studies. These test scans were done with 30 mA, 50 mA, 80 mA and 400 mA (120 kV, rotation time 0.35 s) for the phantom without respiratory motion. Based on the balance between the image quality and radiation dose of these test scans, a 30 mA current was selected for the patient scans. After the ECG-gated CT a 30-min dual gated PET scan was acquired. Finally, a dynamic CT attenuation correction (CTAC) scan with 120 kV and 30 mA was performed. The purpose of this scan was to image respiratory motion.

The motion correction methods were also tested in three patient studies. The subjects (one woman and two men, aged between 62 and 76 years) with diagnosed acute coronary syndrome were studied either prior or after invasive coronary angiography. They followed a very high fat, low-carbohydrate, protein-permitted diet on the previous day of the examination to minimise their myocardium  $^{18}\text{F}$ -FDG uptake and to emphasise the coronary plaque uptake. The  $^{18}\text{F}$ -FDG injection was given 120 min before the dual-gated PET scan in the separate patients' room.

The scanning field-of-view was restricted around the heart and aorta. The imaging protocol for the patient study consisted of a low-dose dynamic ECG-gated CT scan (120 kV, 30 mA, rotation time 0.35 s) during an end-expiratory breath hold, a 30-min dual gated  $^{18}\text{F}$ -FDG-PET scan and a dynamic respiratory gated CTAC scan (120 kV, 30 mA), which had a time duration 1-s longer than the patient's average breathing cycle. Before the ECG-gated CT, a contrast enhanced coronary CT angiography (CTA) was taken for diagnostic purposes. The ECG-gated CT was scanned as soon as possible after the CTA to utilise the contrast agent enhancement in the myocardium. During CT and PET scans the respiratory signal was measured with a breathing mask connected to a spirometer (S/5

anesthesia monitor, GE Healthcare) and the cardiac signal by ECG monitor (Cardiac Trigger Monitor 3150, IVY Biomedical Systems, Inc.). The radiation dose from the study protocol was less than 4 mSv from the low-dose ECG-gated CT, approximately 7 mSv from the PET (370 MBq) and 3-5 mSv from the dynamic CTAC, totalling to less than 16 mSv.

## *2.2 Dual gating of PET data*

During image acquisition both cardiac and respiratory cycles were triggered in real time. Respiratory gating can be implemented with respect to phase or amplitude of the gating signal, i.e., time-based or displacement gating, respectively. Each cycle can be divided into gates with respect to the beginning of the cycle or some predetermined interval from the beginning of the cycle.

For cardiac applications, displacement gating has been shown to be superior compared to time gating [23], so it was also chosen here to divide the respiratory cycle into 5 bins with equal height. The thresholds for the bins were determined using the entire respiratory data from a single acquisition.

Wang et al has shown [5] that the length of the systolic phase of the cardiac cycle is constant when studied in rest. Since only the diastolic phase varies with the heart rate, time based gating can be used to divide the pulsatile motion into gates. Here each ECG cycle was divided into 10 gates with equal length.

In summary we divided the original PET data into 50 gates: 5 respiratory and 10 pulsatile gates. The CT data were gated using the same gating schemas as for the PET data.

### *2.3 Reconstruction of PET data*

The PET images were reconstructed using a software package called Research Gating Toolbox (RGT) provided by GE Healthcare. The software was running in MATLAB (MathWorks, 2009B) programming environment. Iterative 3D OSEM algorithm was used with 35-cm axial field-of-view, two iterations, 28 subsets and Gaussian post-filtering. The matrix of reconstructed images was  $256 \times 256 \times 47$  with voxel size of  $1.37 \times 1.37 \times 3.27$  mm. For attenuation correction, dynamic respiratory gated CTAC images were used [21].

### *2.4 Pre-processing before image registration*

All CT and PET data sets were four dimensional dynamic image series. The matrix size of the ECG-gated and the respiratory-gated CT images were  $512 \times 512$ . For respiratory gating the voxel size was  $0.70 \times 0.70$  mm and slice-separation 2.5 mm and for ECG-gating the voxel size was  $0.49 \times 0.49$  mm and slice-separation 0.63 mm. In order to speed-up the computation and decrease memory requirements, these images were subsampled to a matrix size of  $256 \times 256$ . A mean of the ECG-gated low-dose CT image set was computed. This image set established a reference image set to which all the ECG-gated CT frames were registered. In order to be able to combine the pulsatile motion

correction and respiratory motion correction, and to correct the dual gated PET image sets, all these image sets were transformed to the same coordinate system as the ECG-gated CT image set. The transformation was done using the patient location information available in the image headers [24].

### *2.5 Motion correction algorithms*

Our first method, which is based on motion information calculated solely from gated CT images, is referred to as “CT-only method”. In this method two gated CT scans and one dual-gated PET scan are acquired (Figure 1). The first CT scan is pulsatile gated and the second CT scan is respiratory gated. Pulsatile gating in the first CT scan and in the PET scan are based on the ECG signal. Respiratory gating of the PET scan and the second CT scan are carried out by using a spirometer signal.

Respiratory motion in the dual gated PET images is corrected by using the motion model derived from the respiratory gated CT. This model is created by using an advanced image registration method (Subsection 2.6). Similarly, the pulsatile motion of the respiratory compensated PET images is corrected with help of the motion model derived using an ECG-gated CT and our registration model (Subsection 2.6).

Additionally, a second motion correction method called as “CT-PET-based method” (Figure 2) was also implemented. In this method the respiratory motion is corrected similarly than in CT-only method. However the pulsatile motion is corrected with an image-based method using directly ECG-gated PET images and our image based registration method.

To test the effect of the pulsatile motion correction methods, the respiratory only corrected PET images were also analysed. These images will be referred to as “respiratory corrected”.

A third method, where both pulsatile and respiratory motions were corrected using directly only dual gated PET images and the image based registration algorithm, was also tested.

### *2.6 Image registrations and motion correction*

There may be a miss-alignment between the ECG-gated CT, the respiratory-gated CT and dual gated PET images, e.g., due to the patient body movement. This miss-alignment was corrected with a rigid registration performed between the mean of ECG-gated CT and the respiratory-gated CT. Respiratory frame 4 was selected as the reference frame because it corresponded to the end-expiratory breath-holding phase where also the ECG-gated CT was acquired. The parameters of the rigid transformation were optimised by maximising the normalised mutual information (NMI) using a gradient optimisation. After that, the mean ECG-gated CT image was non-rigidly registered with each frame of the dynamic ECG-gated CT image series. For the non-rigid registration diffeomorphic non-rigid registration method was used. Then the cardiac motion correction could be performed by applying the inverse transformation of the produced correction matrix (see Figure 1, the matrix  $T_P$ ) to the dual gated PET image. For details on the non-rigid registration method, we refer to [25] where it was evaluated in the segmentation of brain structures.

Similarly, the respiratory motion model was obtained by non-rigidly registering the end-expiratory frame 4 of the respiratory-gated CT to each frame of respiratory-gated CT

series. The respiratory motion correction was executed by applying the inverse transformation of the correction matrix (see Figure 1 and 2, the matrix  $T_R$ ) to the PET data.

In the “CT-PET-based” method (see Figure 2) using the respiratory correction matrix  $T_R$ , the dual gated PET images were respiratory corrected. Then the mean images of five respiratory corrected PET images were computed for each pulsatile phase. Next the first frame of this respiratory corrected PET image series was non-rigidly registered to each single PET frame using the same registration method as used for CT images, and the motion correction was done using the inverse transformation. Finally all dual-corrected PET images were averaged.

In the third motion correction method, the correction was carried out for the dual gated PET images without additional information from the CT images. The same image registration method was utilised as in the other our methods.

### *2.7 Motion analysis*

The performance of the motion correction algorithm can be tested by comparing motion between the gates before and after motion correction. Even though the motion correction removes most of the motion, in practice all of the motion cannot be eliminated.

We analysed the motion between different gates in the original, respiratory corrected, “CT-only” dual-corrected and “CT-PET-based” dual-corrected PET images. Here the respiratory corrected image means the dual-gated image, which is corrected for respiration only. For each image the maximum motion between all 50 gates, between all

10 pulsatile gates within the same respiratory phase and between all 5 respiratory gates within the same pulsatile phase was analysed.

For the phantom study the hot targets were used to study motion between the gates. Two methods were used to find the location of the hot targets: the location of the local maximum and the centre-of-mass of voxels with a value greater than 90% of the local maximum. These methods are referred to as the maximum voxel method (MV) and the 90% method (90%), respectively.

In the patient studies the motion of the centre of mass of the myocardium was analysed. The myocardium was automatically segmented with a threshold-based method so that the volume of the segmented myocardium remained constant in each gate. Some gates had very low statistics, which decreased their segmentation accuracy. Therefore intra-gate movement was also quantified. In those cases, the pulsatile motion was defined by averaging respiratory corrected images over different respiratory gates at each pulsatile phase and comparing the pulsatile motion between these averaged images. The respiratory motion was defined similarly by averaging pulsatile corrected images over different pulsatile gates.

### *2.8 Noise and contrast resolution*

Gating increases noise and by motion correction the aim is to decrease the noise level in images. We calculated CNR of nongated PET, gated PET without motion correction, respiratory corrected, “CT-only” dual-corrected and “CT-PET-based” dual-corrected PET images. In the respiratory corrected image only respiratory motion and in the dual-

corrected image both motions were corrected before a weighted sum image from the 50 gates was calculated. The weights in the summing were proportional to the gate duration.

CNR is defined as

$$\frac{|S_t - S_r|}{\sigma},$$

where  $S_t$  is the mean value of the target region,  $S_r$  is the mean value of the reference region and the image noise  $\sigma$  is the standard deviation of a selected region.

In the phantom study  $S_t$  were the hot targets,  $S_r$  was the interior region of the smaller balloon and  $\sigma$  was computed as the standard deviation of the region  $S_r$ . The hot targets were detected by maximum voxel and 90% methods and myocardium by thresholding.

In the patient studies we used the myocardium as  $S_t$  and a cuboid inside the lung tissue [26] as  $S_r$ . The myocardium was similarly automatically segmented by thresholding as in the case of motion analysis (Section 2.7). The  $\sigma$  was computed as the standard deviation of the  $S_r$ .

### *2.9 Size of the targets*

The ability of motion correction to decrease blurring in PET images was tested by analysing the sizes of hot targets. In the phantom studies, the size of the hot targets in original, respiratory corrected, “CT-only” dual-corrected and “CT-PET-based” dual-corrected PET images were analysed. The sizes were determined as full width at half

maximum (FWHM) and full width at 90% maximum (FW90M) in all three coordinate directions. Before calculating FWHM and FW90M the Gaussian curve was fitted into the data. The actual size of the hot targets was 14 mm<sup>3</sup>.

In the patient studies the thickness of the myocardium was estimated using the PET images. A profile was selected from the original and corrected PET images, a Gaussian curve was fitted to the profile data and the myocardium thickness was approximated as the FWHM of the curve. The profiles were selected manually from the coronal planes.

### **3. Results**

Motion correction of dual gated images did not succeed when only the dual-gated PET images were used. To achieve a sufficient motion reduction the data are required to be divided in a rather large number of gates which results in noisy PET images with low statistics. Image-based motion correction methods do not work with such noisy images (Figure 5). Therefore, quantitative analysis was not carried out with the images created only using the PET data.

#### *3.1 Motion analysis*

In the phantom studies the movement of small hot targets was calculated with respect to their initial location. The total respiratory motion of the phantom was 20 mm and total pulsatile motion approximately 7 mm in reality [3]. Theoretically, if the motion was equally spread in all the gates, with 5 respiratory gates it is possible to detect maximum respiratory motion of 16 mm and with 10 pulsatile gates maximum pulsatile motion of

6.3 mm when the finite voxel size is considered. Detected total, respiratory and pulsatile motions are listed in Table 1 and an example of motion of a hot target is shown in Figure 3.

In patient studies the motion of the myocardium was reduced by both dual-correction methods. The CT-PET-based method works better than the CT-only method for correcting the total motion with Patient 1 and 2. However, in the cases of Patient 2 and 3 the CT-PET-based method increased the respiratory motion compared to respiratory corrected images while it decreased the total motion and pulsatile motion.

When all 50 gates were used in motion detection, the total motion was reduced 22.2-59.4% (23.5-57.1%) after CT-only correction (CT-PET-based correction), respiratory motion 25.3-72.5% (26.1-81.7%) and pulsatile motion 3.4-28.1% (8.8-28.8%). Results are collected in Table 2 and an example of motion is shown in Figure 4.

When considering the intra-gate movement total motion was reduced 39.3-58.3% (52.3-74.7%) after CT-only correction (CT-PET-based correction), respiratory motion 41.1-69.1% (50.3-76.4%) and pulsatile motion 31.4-47.9% (57.7-74.7%). Results are summarised in Table 3.

In Figure 5, examples of the averaged patient images are shown.

### *3.2 Contrast-to-noise ratio analysis*

The CNR was analysed from the nongated PET image (original) and the weighted average images of gated PET (gated), respiratory corrected PET (resp. corr.) and dual-corrected PET with CT-only and CT-PET-based methods.

After dual gating the CNR in the phantom images decreased 8.8-16.3% depending on the analysing method. This effect is caused by the reconstruction algorithm, because low counts in OSEM creates bias [27]. However, after motion correction CNR increased significantly. The CT-only method increased CNR compared to the original PET image 55-77% (68.2% on average) and the CT-PET-based method 69-83% (74.4% on average), see Table 4.

In the patient study the image noise was determined as the standard deviation of pixel values in the myocardium. The CT-only method increased CNR 3.5-8.6% (6.0% on average) and the CT-PET-based method 2.5-9.5% (6.9% on average), see Table 5.

An example of the corrected images from the phantom and patient studies are shown in Figure 6.

### *3.3 Target-size analysis*

In the phantom study the size of hot targets averaged over all targets decreased 40.2% after respiratory correction, 38.3% after CT-only correction and 47.0% after CT-PET-based correction when measured with FWHM. The size of the most active hot target decreased 43.3% after respiratory correction, 21.4% after CT-only correction and 36.6% after CT-PET-based correction in terms of FWHM. Corresponding decreases measured with FW90M were 37.7%, 43.3% and 49.7% averaged over all hot targets and 42.4%, 30.9% and 42.0% for the most active hot target. The results are shown in Table 6.

In patient studies the thickness of the myocardium decreased 5.4-11.7% (9.0% on average) after respiratory correction, 7.9-13.3% (10.3% on average) after CT-only dual-

correction and 16.1-42.1% (27.7% on average) after CT-PET-based dual-correction. The results are listed in Table 7.

#### **4. Discussion**

The aim of this study was to develop a new motion correction method for dual gated cardiac PET. We introduced two methods and tested them with phantom data and patient datasets. Both methods are based on the detection of motion from gated CT images.

We used respiratory and pulsatile gated CT images to create a motion correction model for PET images. In both methods the respiratory motion in PET images was corrected first, because it is larger [28] than the pulsatile motion and the CT image used for respiratory gating has better quality.

To our knowledge there are no studies on the effects of different gating schemes for dual gating in PET. Therefore, we assumed that the best methods for respiratory and pulsatile gating are also the best gating methods for dual gating. In this study the number of gates and the gating methods were pre-selected. Selection of respiratory gating method was based on literature [23].

##### *4.1 Phantom study*

Our heart phantom was specially designed for testing the dual gating protocol and in this study it was used to test the motion correction methods [3]. The motion analysis for the heart phantom gave excellent results as expected, because the motion of phantom was regular and the radioactive targets were uniform.

According to the phantom study the gating and the motion methods work well. The detected total respiratory motion was 12 mm and pulsatile motion 6 mm. The CT-only motion correction method reduced the total motion from 15 to 7 mm and the CT-PET-based method to 6 mm. The difference between the motion correction methods is marginal and both the methods eliminated the motion between gates effectively as compared to the scanner spatial resolution which is between 5 and 6 mm [22]. The detection of the respiratory motion may be further improved by adding the number of respiratory gates. However, in this study the number of gates was fixed to 5. The effect of changing the number of gates should be separately studied.

In the phantom study CNR increased significantly. The CT-only method increased CNR of the radioactive targets 68% compared to the original nongated PET image and 89% compared to the gated PET image. The CT-PET-based method increased CNR 74% compared to the original nongated PET image and 96% compared to the average-of-gated PET image.

Also the target-size decreased considerably in phantom study. The volume of the most active target decreased from 27.4 to 15.5 mm<sup>3</sup> after the CT-only motion correction and to 13.3 mm<sup>3</sup> after the CT-PET-based correction. The real size of the target was 14 mm<sup>3</sup>. These results show that the both motion correction methods work with the small targets (3 mm), when the target to background ratio is large (33-200).

The successful results were anticipated because of the solidity and the small size of the radioactive targets. With the phantom data, it was possible to test whether the motion artefacts of small active targets mimicking coronary plaques can be compensated with our motion correction methods. With the patient data, however, the coronary plaques do not accumulate the <sup>18</sup>F-FDG with such a high ratio as simulated with the phantom data.

Therefore the results achieved with the phantom data do not directly reflect how well the motion correction methods work with the patient data.

#### *4.2 Patient study*

The motion correction methods produced successful results also with the patient data. The motion reduction was measured using two different techniques. When the location of the automatically segmented myocardium from all 50 dual gated images was analysed, the total motion was reduced 22-59% after the CT-only correction and 24-57% after the CT-PET-based correction. When the location of the automatically segmented myocardium from 5 respiratory gated and 10 pulsatile gated images were analysed, the total motion was reduced 39-58% after the CT-only correction and 52-76% after the CT-PET-based correction. Since we used 50 dual gated images in our analyses, some gates had low statistic and the automated segmentation did not work very well with those dual gated images. Therefore the extent of the estimated motion may be unrealistically high in some gates when all 50 dual gates were analysed.

The motion correction only slightly improved the CNR in the patient datasets. The CT-only method increased the CNR of myocardium by 6.0% and the CT-PET-based method 6.9%. First, we tested a VOI from the lungs as the reference region but it turned out that the standard deviation of this region could not be used in the final calculation of CNR (see Sect 4.3). Instead we calculated the standard deviation over the myocardium region.

The motion correction methods improved successfully the spatial resolution of images when applied to the patient datasets. The CT-only method decreased the

myocardium thickness by 10% and the CT-PET-based method by 28%. In this analysis the CT-PET-based method turned out to be superior compared to the CT-only method.

#### *4.3 Properties of motion correction methods*

The results from the heart phantom study are better than those from the patient datasets because the phantom has constant respiratory and cardiac motion, the contrast of the radioactivity targets is higher in the phantom and the motion correction algorithm works more efficiently on the outer boundary of the artificial heart than with the real human heart. The CNR results of the patient datasets are moderate because the myocardium was selected to be the reference region instead of the lung. The reason for this was the very low radioactivity uptake, which distorts a reliable standard deviation calculation in the lung.

One of our main goals in developing the dual gating and the motion correction methods was to improve our tools to detect small anatomical targets close to the heart, such as vulnerable coronary plaques. In patient studies, especially with FDG, the existence of vulnerable coronary plaques was hard to determine even though our patients followed a special diet to minimise the normal myocardium FDG uptake. This is an additional reason why the phantom study produced better results to the patient studies. A recent study suggested that  $^{18}\text{F}$ -NaF is better tracer to identify and localise coronary plaques than  $^{18}\text{F}$ -FDG [2]. Our results achieved with the patient data could have been improved if  $^{18}\text{F}$ -NaF had been used.

The CT-PET-based method gave slightly better results in all three motion analyses. Furthermore the CT-only method requires higher radiation dose and an additional CT

image, whereas the CT-PET-based method does not use any anatomical information from the CT images in the correction of the pulsatile motion. In these perspectives the CT-PET-based method is much more favourable than CT-only method in motion correction. In addition both methods function superiorly compared to the respiratory only correction because the dual-correction methods reduce successfully also the pulsatile motion.

The detection of cardiac motion from the gated images is a demanding task. To simplify this we calculated the movement of centre of mass of the myocardium in our patient study. This approach detects more efficiently a rather rigid respiratory motion, but may not work for the pulsatile motion in which the cardiac activity can even deform around its centre of mass.

#### *4.4 Gating methods*

There are several methods to minimise and detect the respiratory motion during PET imaging. One of the first motion elimination methods was to ask the patient to breath according to breathing instruction [10]. More advanced methods detect the breathing motion using a camera [11], pressure belt [7] or spirometer [29, 30]. There are also methods that create the respiratory signal directly from the PET list mode data without any auxiliary equipment [31, 32, 33, 34, 35]. Several methods are also used to detect the cardiac motion, the most commonly used being ECG. In this study we used spirometer for respiratory gating and ECG for pulsatile gating. Both methods suited excellently for gating and patients tolerated well the breathing mask used with the spirometer.

In our motion correction methods the motion model of the heart is created utilising CT images. The optimal model could be created using dual gated CT images. However,

the acquisition of dual gated CT data was not technically or ethically possible, because it would have produced high radiation dose to the patient. In addition, our ECG-gated CTs had a non-optimal contrast agent enhancement because the contrast agent was given during the actual CTA examination taken beforehand for the diagnostic purposes. If the injection of contrast agent would have been optimally scheduled with the ECG-gated CT, the myocardium segmentation in the gated CTs would have been improved especially between the border of myocardium and liver.

Our CT-only motion correction method can be used even if the PET images have low statistics. Therefore, the method makes it possible to execute the gating with a high amount of gates. In this study the method worked successfully with 50 gates.

The number of gates used in the study was fixed. The number of pulsatile gates was first fixed because our method utilised the gates with an equal length and our tests showed that 10 pulsatile gates were needed to detect pulsatile motion with a reasonable resolution. Secondly, the number of respiratory gates was fixed. Literature suggests that 8 respiratory gates would be an optimal number for respiratory gating. We compromised this to 5 to ensure that each dual gate would contain enough data.

#### *4.5 Motion correction with large number of gates*

Several motion correction methods for respiratory gated cardiac PET have been published [13, 17, 18, 23, 31, 34]. Dawood et al [13] reported that their optical flow method reduced respiratory motion from 9.9 to 2.6 mm (74%) in patient studies and over 90% in a phantom study. However, no quantitative results after correcting the pulsatile motion of heart from cardiac PET images have been published. The larger respiratory

motion is technically easier to correct than the smaller pulsatile motion [28]. Gigengack et al [6] published the motion correction method for dual gated cardiac PET. They used mass preserving image registration, which is solely image based method. Their method reduced the cardiac motion analysed using the centre of mass from  $5.8\pm 3.4$  to  $0.7\pm 0.2$  mm.

We compared our novel CT-based method with a motion correction method, which uses only PET images. We used method similar to [6] and it did not manage to correct the motion artefacts in our tests, because the dual gated PET images were too noisy after gating. The only way to overcome this problem is to reduce the number of dual gates and it would limit the motion that could be detected. We used 50 dual gates, whereas Dawood et al. used 8 respiratory gates [13] and Gigengack et al. 25 dual gates (5 respiratory and 5 pulsatile gates) [6].

#### *4.6 Features of our motion correction methods*

Our novel motion correction methods have disadvantages that are typical for PET/CT scans. Because the PET and CT scans are acquired sequentially the patient can move between the scans causing rigid motion artefacts between the CT and PET images. These rigid motion artefacts need to be corrected first before applying CT based methods into the data.

In our motion correction methods the CT scans cover only a few respiratory and pulsatile cycles whereas the PET images are averaged over the entire 30-min scan. In patient studies the magnitude and rate of respiratory and pulsatile motion can vary. Therefore the heart does not necessarily move exactly similarly in the CT and PET

images causing a potential inaccuracy in the correction methods. Also the quality of the respiratory and pulsatile gated CT images differ and there is attenuation mismatch, which causes artefacts in reconstructed PET images.

Both CT-only and CT-PET-based methods are fully automated. The computation of each non-rigid registration requires currently about 4-min per gate with normal desktop computer (2.50 GHz processor, 4.00 GB RAM). The pre-processing steps take additional 5 to 10 min, and the motion corrections about 10 min. The total process at the moment takes about 4 hours per a study. The computation time can be quite easily shortened to less than a half an hour by combining the separate software blocks and optimising the code. In addition more powerful computer and parallel computing could be used to further speed-up our algorithms substantially by simultaneously registering multiple images.

In this work, a non-rigid registration algorithm described in [25] was used. However, other non-rigid registration tools able to align two volumetric intensity images accurately could be used as well.

A problem with the current implementation of the methods is that the dual-gated data are count-starved. Iterative image reconstruction algorithms are known to have positive bias in such cases [27]. However, this can be overcome by using the estimated motion during reconstruction of all gates simultaneously as shown for respiratory gating in [36]. This would be easiest to realise with the CT-only method. For the CT-PET method, the data would have to be re-reconstructed after the cardiac motion is derived from the initial reconstructed PET images.

The main disadvantage of our motion correction methods is the increased radiation dose due to the additional CT scans. The radiation dose can be decreased by using the

new CT techniques such as iterative reconstruction algorithms and novel detector materials [37, 38]. In future also PET/MRI scanner could be used for imaging cardiac motion instead of PET/CT scanner. This would solve the problem of additional radiation dose and would increase the soft tissue contrast in the anatomical cardiac images. There are preliminary studies of MR based motion correction methods for PET images [39, 40] and the next step is to develop our motion correction method from PET/CT to PET/MR.

## **5. Conclusions**

Two novel motion correction algorithms were developed and applied to cardiac phantom and patient datasets. These methods result several advantages improving spatial resolution and contrast so that smaller targets can be distinguished in PET images. The use of these motion correction algorithms could lead to patient studies with better diagnostic accuracy, shorter imaging time and/or lower injected dose.

## References

- [1] G. Delso, A. Martinez-Möller, R.A. Bundschuh, S.G. Nekolla, S.I. Ziegler, M. Schwaiger. Preliminary studies of the detectability of coronary plaque with PET. *Phys Med Biol* 2011; 56 (7): 2145-60.
- [2] N.V. Joshi, A.T. Vesey, M.C. Williams, A.S.V. Shah, P.A. Calvert, F.H.M. Craighead *et al.* 18F-fluoride positron emission tomography for identification of ruptured and high-risk coronary atherosclerotic plaques: a prospective clinical trial. *Lancet* 2014; 383 (9918): 705-713.
- [3] T. Kokki, H.T. Sipilä, M. Teräs, T. Noponen, N. Durand-Schaefer, R. Klén *et al.* Dual gated PET/CT for imaging of vulnerable coronary plaques: Method description and testing with a dynamic heart phantom. *J Nucl Cardiol* 2009; 17: 71-84.
- [4] A.J. Schwarz, M.O. Leach. Implications of respiratory motion for the quantification of 2D MR spectroscopic imaging data in the abdomen. *Phys Med Biol* 2000; 45 (8): 2105-2116.
- [5] Y. Wang, E. Vidan, G. W. Bergman. Cardiac motion of coronary arteries: variability in the rest period and implications for coronary MR angiography. *Radiology* 1999; 213: 751-58.
- [6] F. Gigengack, L. Ruthotto, M. Burger, C.H. Wolters, X. Jiang, K.P. Schäfers. Motion

Correction in Dual Gated Cardiac PET using Mass-Preserving Image Registration. *IEEE Trans Med Imaging* 2012; 31 (3): 698-712.

[7] A. Martinez-Möller, D. Zikic, R.M. Botnar, R.A. Bundschuh, W. Howe, S.I. Ziegler *et al.* Dual cardiac-respiratory gated PET: implementation and results from a feasibility study. *Eur J Nucl Med Mol Imaging* 2007; 34: 1447-1454.

[8] M. Teräs, T. Kokki, N. Durand-Schaefer, T. Noponen, M. Pietilä, J. Kiss *et al.* Dual-gated cardiac PET-Clinical feasibility study. *Eur J Nucl Med Mol Imaging* 2010; 37 (3): 505-16.

[9] N. Lang, M. Dawood, F. Büther, O. Schober, K. Schäfers. Organ Movement Reduction in PET/CT using Dual-Gated Listmode Acquisition. *Z Med Phys* 2006; 16: 93-100.

[10] G.W. Goerres, E. Kamel, T.-N.H. Heidelberg, M.R. Schwitter, C. Burger, G.K. von Schulthess. PET-CT image co-registration in the thorax: influence of respiration. *Eur J Nucl Med* 2002; 29 (3): 351-360.

[11] S.A. Nehmeh, Y.E. Erdi, C.C. Ling, K.E. Rosenzweig, H. Schoder, S.M. Larson *et al.* Effect of Respiratory Gating on Quantifying PET Images of Lung Cancer. *J. Nucl. Med.* 2002; 43 (7): 876-881.

- [12] F. Lamare, T. Cresson, J. Savean, C. Cheze Le Rest, A.J. Reader, D. Visvikis. Respiratory motion correction for PET oncology applications using affine transformation of list mode data. *Phys Med Biol* 2007; 52: 121-140.
- [13] M. Dawood, F. Büther, X. Jiang, K.P. Schäfers. Respiratory Motion Correction in 3-D PET Data With Advanced Optical Flow Algorithms. *IEEE Trans Med Imag* 2008; 27 (8): 1164-1175.
- [14] M. Dawood, N. Lang, X. Jiang, K.P. Schäfers. Lung Motion Correction on Respiratory Gated 3-D PET/CT Images. *IEEE Trans Med Imag* 2006; 25 (4): 476-485.
- [15] G.J. Klein, B.W. Reutter, R.H. Huesman. Non-Rigid Summing of Gated PET Via Optical Flow. *IEEE Trans Nucl Sci* 1997; 44 (4): 1509-1512.
- [16] F. Lamare, M.J. Ledesma Carbayo, T. Cresson, G. Kontaxakis, A. Santos, C. Cheze Le Rest *et al.* List-mode-based reconstruction for respiratory motion correction in PET using non-rigid body transformations. *Phys Med Biol* 2007; 52: 5187-5204.
- [17] A.J. Chung, P.G. Camici, G.-Z. Yang. List-Mode Affine Rebinning for Respiratory Motion Correction in PET Cardiac Imaging. *Lecture notes in computer science* 2006; 4091: 293-300.

- [18] A.J. Chung, P.G. Camici, G.-Z. Yang. Cardiac PET Motion Correction Using Materially Constrained Transform Models. *Lecture notes in computer science* 2008; 5128: 193-201.
- [19] S. Ambwani, S. Cho, W.C. Karl, A. Tawakol, H. Pien. A Feasibility Study of Joint Respiratory and Cardiac Motion Correction for Coronary PET/CT Imaging. *ISBI'09: Proceedings of the Sixth IEEE international conference on Symposium on Biomedical Imaging* 2009: 935-938.
- [20] F. Lamare, A. Le Maitre, M. Dawood, K.P. Schäfers, P. Fernandez, O.E. Rimoldi, D. Visvikis. Evaluation of respiratory and cardiac motion correction schemes in dual gated PET/CT cardiac imaging. *Med Phys* 2014; 41: 072504.
- [21] A.M. Alessio, S. Kohlmyer, K. Branch, G. Chen, J. Caldwell, P. Kinahan. Cine CT for Attenuation Correction in Cardiac PET/CT. *J Nucl Med* 2007; 48 (5): 794-801.
- [22] M. Teräs, T. Tolvanen, J.J. Johansson, J.J. Williams, J. Knuuti. Performance of the new generation of whole-body PET/CT scanners: Discovery STE and Discovery VCT. *Eur J Nucl Med Mol Imaging* 2007; 34 (10): 1683-92.
- [23] M. Dawood, F. Büther, N. Lang, O. Schober, K.P. Schäfers. Respiratory gating in positron emission tomography: A quantitative comparison of different gating schemes. *Med Phys* 2007; 34 (7): 3067-3076.

- [24] J. Lötjönen, M. Pollari, S. Kivistö, K. Lauerma. Correction of Motion Artifacts From Cardiac Cine Magnetic Resonance Images. *Acad Radiol* 2005; 12: 1273-128.
- [25] J.M. Lötjönen, R. Wolz, J.R. Koikkalainen, L. Thurffjell, G. Waldemar, H. Soininen *et al.* Fast and robust multi-atlas segmentation of brain magnetic resonance images. *Neuroimage* 2010; 49: 2352-2365.
- [26] M. Dawood, F. Büther, L. Stegger, X. Jiang, O. Schober, M. Schäfers *et al.* Optimal number of respiratory gates in positron emission tomography: A cardiac patient study. *Med Phys* 2009; 36 (5): 1775-1784.
- [27] M.D. Walker, M.C. Asselin, P.J. Julyan, M. Feldmann, P.S. Talbot, T. Jones *et al.* Bias in iterative reconstruction of low-statistics PET data: benefits of a resolution model. *Phys Med Biol* 2011; 56 (4): 931-49.
- [28] K. McLeish, D.L.G. Hill, D. Atkinson, J.M. Blackall, R. Razavi. A study of the motion and deformation of the heart due to respiratory. *IEEE Trans Med Imaging* 2002; 21: 1142-1150.
- [29] T.Z. Zhang, H. Keller, M.J. O'Brien, T.R. Mackie, B. Paliwal. Application Of The Spirometer In Respiratory Gated Radiotherapy. *Med Phys* 2003; 30 (12): 3165-3171.

- [30] T. Noponen, T. Kokki, V. Lepomaki, S. Kajander, N. Durand-Schaefer, M. Teräs *et al.* Spirometry based respiratory gating method for cardiac PET and MRI imaging. *Nuclear Science Symposium Conference Record* 2008: 4832-4834.
- [31] F. Büther, M. Dawood, L. Stegger, F. Wübbeling, M. Schäfers, O. Schober *et al.* List Mode-Driven Cardiac and Respiratory Gating in PET. *J Nuc Med* 2009; 50 (5): 674-681.
- [32] A.L. Kesner, P.J. Schleyer, F. Büther, M.A. Walter, K.P. Schäfers, P.J. Koo. On transcending the impasse of respiratory motion correction applications in routine clinical imaging – a consideration of a fully automated data driven motion control framework. *EJNMMI Physics* 2014, 1:8.
- [33] G.J. Klein, B.W. Reutter, E.H. Botvinick, T.H. Budinger, R.H. Huesman. Fine-scale motion detection using intrinsic list mode PET information. *Mathematical Methods in Biomedical Image Analysis* 2001: 71-78.
- [34] P.J. Schleyer, M.J. O’Doherty, S.F. Barrington, P.K. Marsden. Retrospective data-driven respiratory gating for PET/CT. *Phys Med Biol* 2009; 54: 1935-1950.
- [35] K. Thielemans, S. Rathore, F. Engbrant, P. Razifar. Device-less gating for PET/CT using PCA. *Nuclear Science Symposium and Medical Imaging Conference* 2011: 3904-3910.

- [36] I. Polycarpou, C. Tsoumpas, P.K. Marsden. Analysis and comparison of two methods for motion correction in PET imaging. *Med Phys* 2012; 39: 6474-6483.
- [37] M. Fiechter, J.R. Ghadri, S.M. Kuest, A.P. Pazenkottl, M. Wolfrum, R.N. Nkoulou *et al.* Nuclear myocardial perfusion imaging with a novel cadmium-zinc-telluride detector SPECT/CT device: first validation versus invasive coronary angiography. *Eur J Nucl Med Mol Imaging* 2010; 38 (11): 2025-2030.
- [38] A.K. Hara, R.G. Paden, A.C. Silva, J.L. Kujak, Holly J. Lawder, and W. Pavlicek. Iterative Reconstruction Technique for Reducing Body Radiation Dose at CT: Feasibility Study. *Am J Roentgenol* 2009; 193 (3): 764-71.
- [39] Y. Petibon, G. El Fakhri, R. Nezafat, N. Johnson, T. Brady, J. Ouyang. Towards coronary plaque imaging using simultaneous PET-MR: a simulation study. *Phys Med Biol* 2014; 59: 1203-22.
- [40] C. Würslin, H. Schmidt, P. Martirosian, C. Brendle, A. Boss, N.F. *et al.* Respiratory Motion Correction in Oncologic PET Using T1-Weighted MR Imaging on a Simultaneous Whole-Body PET/MR System. *J Nucl Med* 2013; 54 (3): 464-471.

## CT-only method

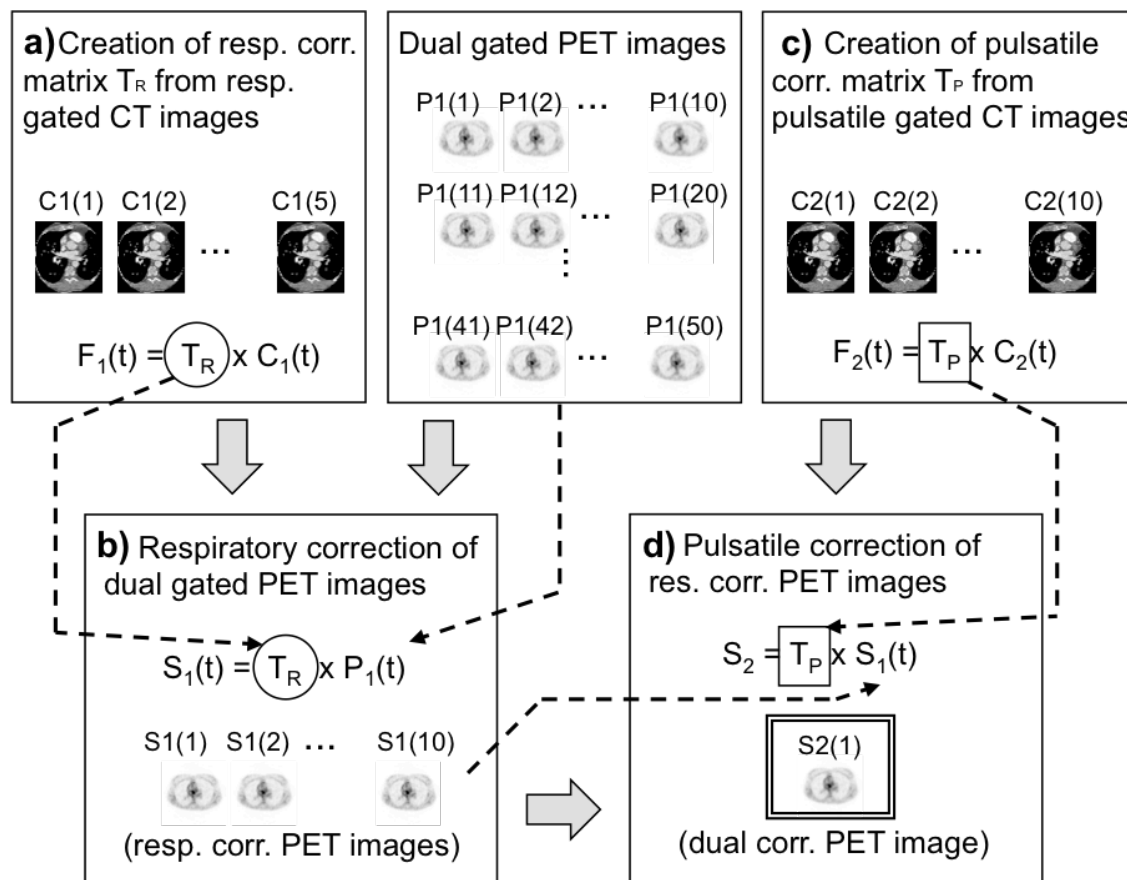


Figure 1. CT-only method. a) The respiratory gated CT images  $C_1(t)$  are used to create a respiratory motion correction matrix  $T_R$ . b) The matrix  $T_R$  is then applied to create respiratory corrected PET images  $S_1(t)$  from the dual gated PET images  $P_1(t)$ . c) The pulsatile gated CT images  $C_2(t)$  are used to create a pulsatile motion correction matrix  $T_P$ . d) The pulsatile correction for the respiratory corrected PET images  $S_1(t)$  is implemented by using the matrix  $T_P(t)$ . The result is the motion corrected PET image  $S_2$ .

## CT-PET based method

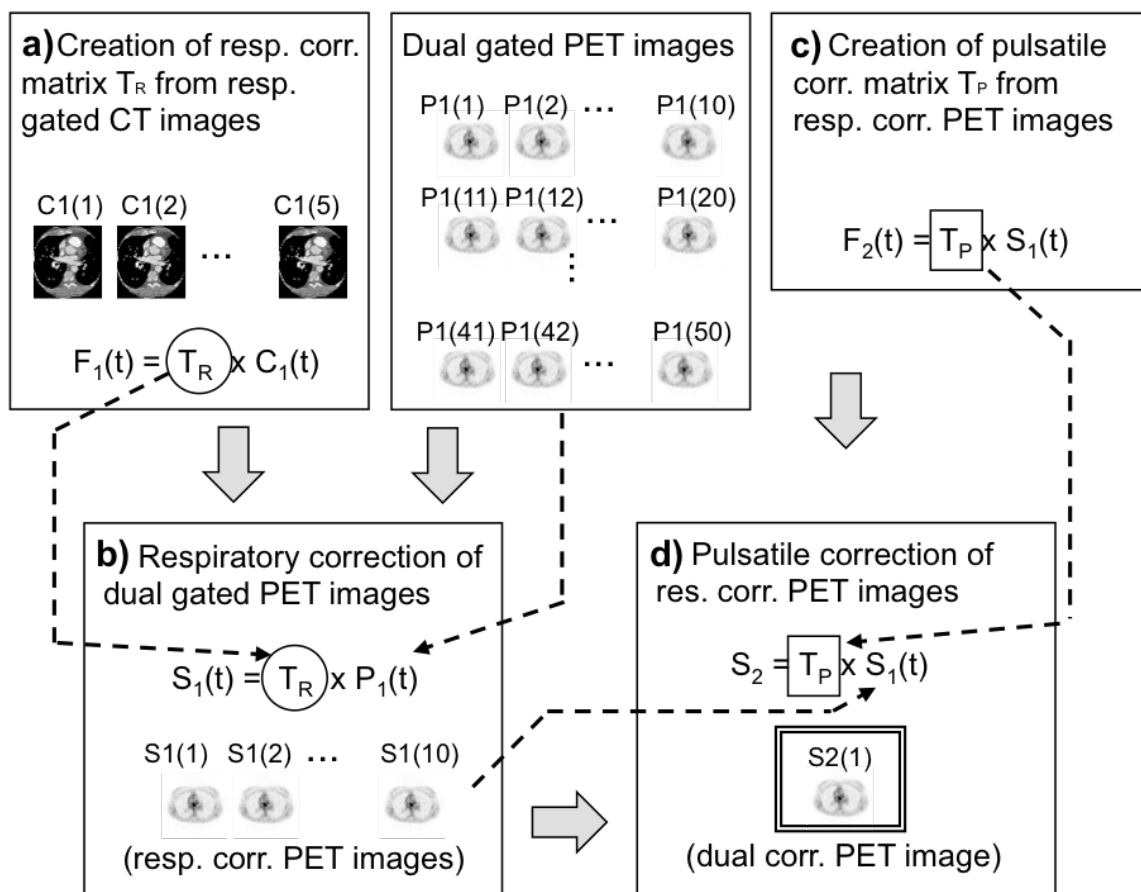


Figure 2. CT-PET-based method. a) The respiratory gated CT images  $C_1(t)$  are used to create a respiratory motion correction matrix  $T_R$ . b) The matrix  $T_R$  is then applied to create respiratory corrected PET images  $S_1(t)$  from the dual gated PET images  $P_1(t)$ . c) The respiratory corrected PET images  $S_1(t)$  are used to create a pulsatile motion correction matrix  $T_P$ . d) The pulsatile correction for the respiratory corrected PET images  $S_1(t)$  is implemented by using the matrix  $T_P(t)$ . The result is motion corrected PET image  $S_2$ .

Table 1. Motion of hot targets in the phantom study before any corrections (original), after respiratory, CT-only dual- and CT-PET-based dual-correction.

All hot targets	original (mm)	resp. corr. (mm)	CT-only (mm)	CT-PET-based (mm)
total motion (MV)	15.3	8.6	6.6	5.9
total motion (90%)	14.9	8.5	7.3	5.8
resp. motion (MV)	12.2±0.7	4.4±0.5	4.5±0.6	4.2±0.5
resp. motion (90%)	12.1±0.6	4.3±0.5	4.7±0.6	4.4±0.4
puls. motion (MV)	5.9±0.2	5.5±0.5	2.9±0.4	2.0±0.5
puls. motion (90%)	5.8±0.2	5.4±0.3	2.9±0.3	1.7±0.3

Most active hot target	original (mm)	resp. corr. (mm)	CT-only (mm)	CT-PET-based (mm)
total motion (MV)	14.4	6.9	4.5	4.5
total motion (90%)	14.1	6.3	5.7	3.6
resp. motion (MV)	12.1±1.6	3.7±0.1	3.6±0.1	3.8±0.2
resp. motion (90%)	12.3±1.3	3.6±0.1	4.2±0.7	3.5±0.03
puls. motion (MV)	6.3±0.4	5.2±0.7	2.2±0.5	1.6±0.3
puls. motion (90%)	5.3±0.4	4.6±0.6	2.2±0.4	1.0±0.4

The location of the hot targets was detected by two different methods: maximum voxel (MV) and 90% methods. In both cases the mean of the detected displacement of all hot targets and the displacement of the most active hot target were analysed. The error values are standard deviations over targets.

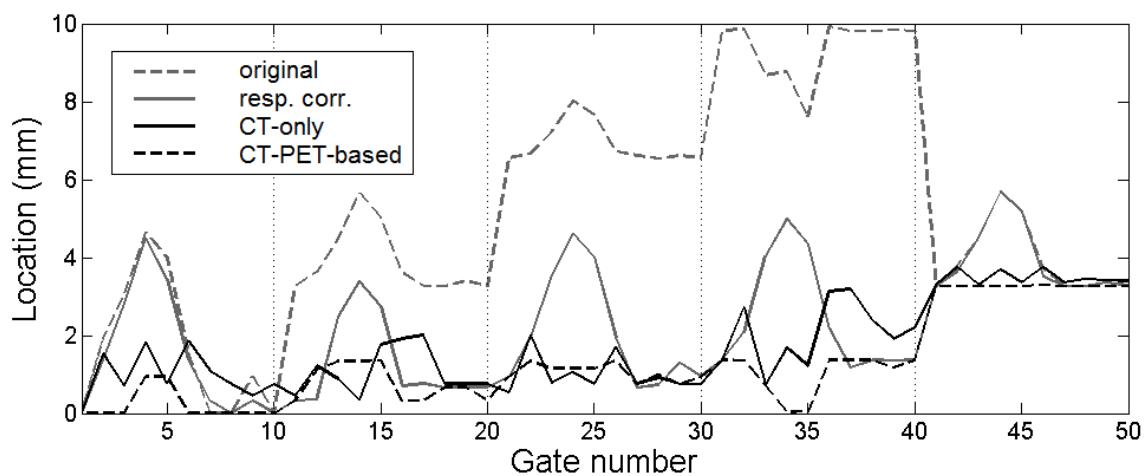


Figure 3. Motion of a hot target in the phantom study. Dashed grey line is the location of a hot target in the original gated image, solid grey line after respiratory correction, solid black line after CT-only correction and dashed black line after CT-PET-based correction.

Table 2. Motion of the myocardium in the dual-gated patient images.

Patient 1	original (mm)	resp. corr. (mm)	CT-only (mm)	CT-PET-based (mm)
total motion	18.6	14.7	14.5	11.3
respiratory motion	14.5±2.3	10.9±2.1	10.8±1.8	8.6±1.1
pulsatile motion	6.9±1.8	6.9±1.7	6.6±1.7	4.7±0.7
Patient 2	original (mm)	resp. corr. (mm)	CT-only (mm)	CT-PET-based (mm)
total motion	13.2	7.6	6.8	5.5
respiratory motion	9.7±0.6	2.7±0.5	2.7±0.5	3.0±0.8
pulsatile motion	6.7±0.8	6.2±0.8	5.6±0.6	3.5±0.8
Patient 3	original (mm)	resp. corr. (mm)	CT-only (mm)	CT-PET-based (mm)
total motion	25.8	13.8	10.5	11.5
respiratory motion	18.5±1.4	7.4±1.3	6.8±1.0	8.2±1.1
pulsatile motion	9.8±1.15	8.3±1.3	7.1±0.9	5.1±1.6

The results are calculated as the maximum motion between two gates.

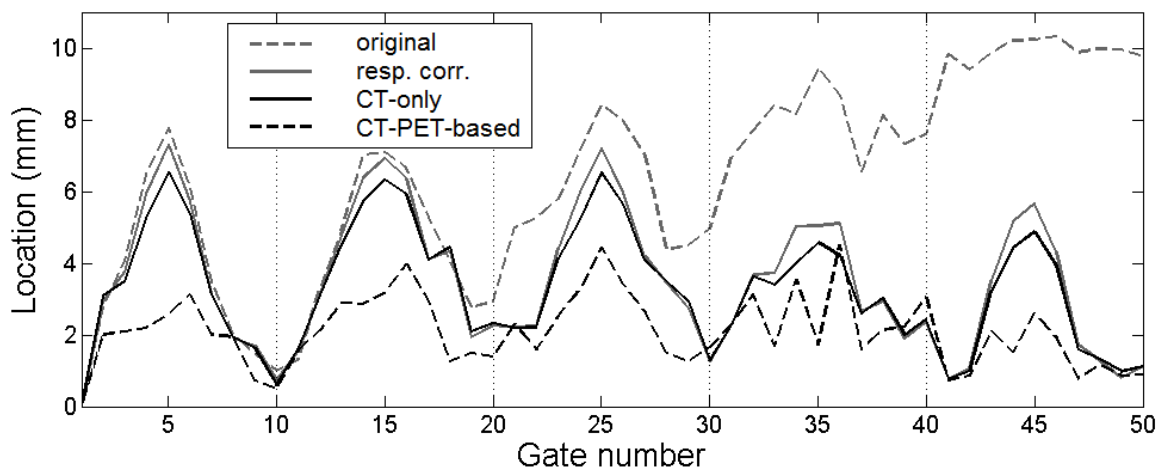


Figure 4. The location of centre-of-mass of myocardium FDG-activity with respect to its initial location in a patient study (Patient 2). Dashed grey line is the location in the original gated image, solid grey line after respiratory correction, solid black line after CT-only correction and dashed black line after CT-PET-based correction.

Table 3. Intra-gate movement in the patient studies.

Patient 1	original (mm)	resp. corr. (mm)	CT-only (mm)	CT-PET-based (mm)
respiratory motion	14.4	10.1	10.2	7.2
pulsatile motion	5.5	5.2	5.0	2.3
Patient 2	original (mm)	resp. corr. (mm)	CT-only (mm)	CT-PET-based (mm)
respiratory motion	9.4	1.7	1.7	2.2
pulsatile motion	6.1	5.6	4.9	1.7
Patient 3	original (mm)	resp. corr. (mm)	CT-only (mm)	CT-PET-based (mm)
respiratory motion	17.2	5.6	5.5	6.3
pulsatile motion	9.9	8.5	7.1	2.5

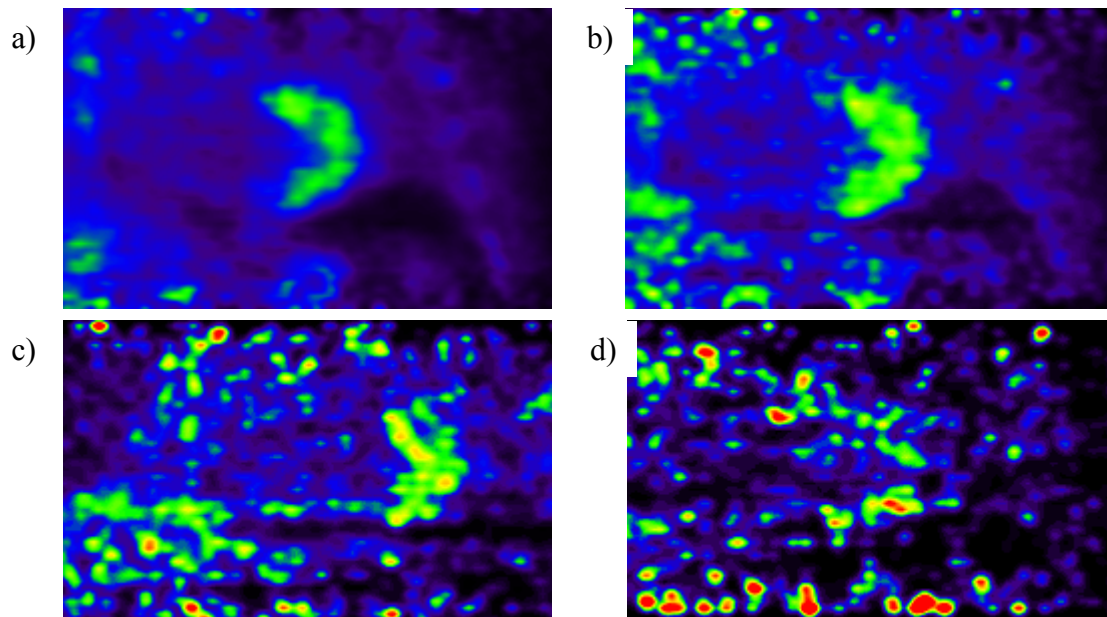


Figure 5. a) Average image of 50 dual-gated PET images. b) Average image over 10 pulsatile gated PET images during one respiratory phase. c) A good quality dual-gated PET image. d) A moderate quality dual-gated PET image.

Table 4. CNRs in the phantom study.

CNR	original	gated	resp. corr.	CT-only	CT-PET-based
1 hot spot, MV	667	605	986	1150	1157
1 hot spot, 90%	625	570	933	1106	1141
mean, MV	380	344	546	640	644
mean, 90%	372	311	531	576	641

CNR of nongated (original), average-of-gated (gated), respiratory and dual-corrected PET images in the phantom study. The hot targets were detected by the maximum voxel (MV) and the 90% methods. The CNR was computed for the most active target (one target) and as an average over all hot targets (mean).

Table 5. CNRs in the patient studies.

CNR	original	gated	resp. corr.	CT-only	CT-PET-based
patient 1	8.17	8.82	8.91	8.87	8.94
patient 2	11.9	11.7	12.9	12.6	12.9
patient 3	4.45	4.65	4.69	4.60	4.56

CNR of nongated (original), average-of-gated (gated), respiratory and dual-corrected PET images from the patient studies.

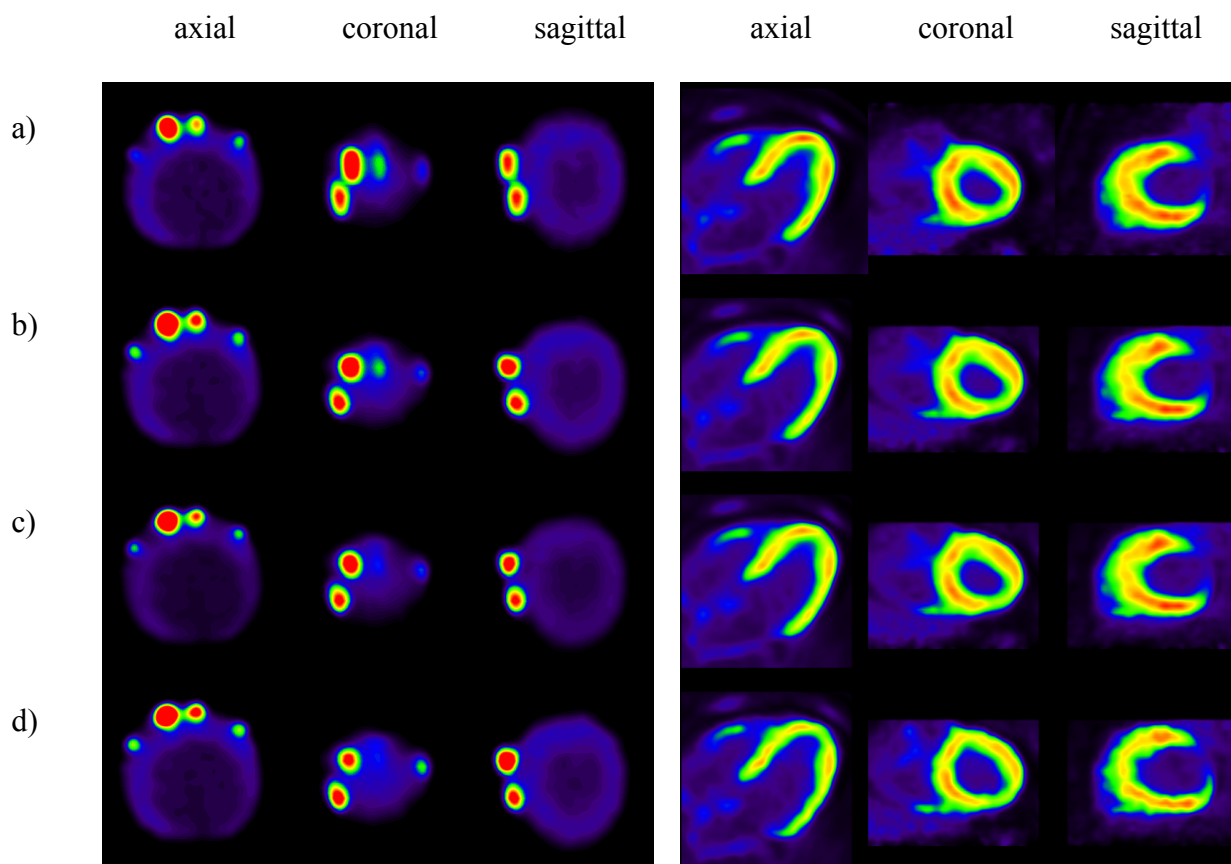


Figure 6. Hot targets in the phantom study (left) and the myocardium from the patient 2 (right). (a) The nongated, (b) the respiratory corrected, (c) the CT-only dual-corrected, and (d) the CT-PET-based dual-corrected image. The left column is transaxial, the middle coronal and the right sagittal view.

Table 6. Volumes of hot targets in the phantom study.

Volume (FW90M)	mean (mm <sup>3</sup> )	most active (mm <sup>3</sup> )
original image	22.5±4.7	27.4
respiratory corrected	14.0±2.4	12.9
CT-only dual corrected	12.7±2.6	15.5
CT-PET-based dual corrected	11.3±1.8	13.1
Volume (FWHM)		
original image	449±86	519
respiratory corrected	268±49	254
CT-only dual corrected	276±70	352
CT-PET-based dual corrected	238±45	284

The volume of the most active hot target (most active) and the average value of all hot targets (mean) are given. The volumes were defined from the PET images with FWHM and FW90M methods. The actual size of the hot targets is 14 mm<sup>3</sup>.

Table 7. Myocardium thickness estimated from the PET images.

Myocardium thickness	original image (mm)	respiratory corrected (mm)	CT-only corrected (mm)	CT-PET based corrected (mm)
patient 1	16.4	15.5	15.1	9.5
patient 2	17.4	15.7	15.7	14.6
patient 3	24.0	21.2	20.8	18.0

A profile was determined in the coronal slice and FWHM was calculated from a fitted Gaussian.